

Rapidity dependence of hadron production in central Au+Au collisions at $\sqrt{s_{NN}} = 200$ GeV

Jun Song,¹ Feng-lan Shao,¹ Qu-bing Xie,² Yun-fei Wang,¹ and De-ming Wei¹

¹*Department of Physics, Qufu Normal University, Shandong 273165, People's Republic of China*

²*Department of Physics, Shandong University, Shandong 250100, People's Republic of China*

The rapidity and transverse momentum spectra for identified hadrons in central Au+Au collisions at $\sqrt{s_{NN}} = 200$ GeV are computed in a quark combination model. The data of rapidity distributions for π^\pm , K^\pm , $p(\bar{p})$ and net protons ($p - \bar{p}$) are well described. We also predict rapidity distributions for K_s^0 , $\Lambda(\bar{\Lambda})$, $\Xi^- (\bar{\Xi}^+)$ and $\Omega^- + \bar{\Omega}^+$. The multiplicity ratios of charged antihadrons to hadrons as a function of rapidity are reproduced. The results for p_T spectra of π^\pm , K^\pm , $p(\bar{p})$ and for the p/π ratios in a broader p_T range agree well with the data. Finally the rapidity dependence of transverse momentum distributions for hadrons are given.

PACS numbers: 25.75.Dw, 25.75.-q

I. INTRODUCTION

The relativistic heavy ion collider (RHIC) at Brookhaven National Lab (BNL) provides a unique environment to search for the quark gluon plasma (QGP) predicted by lattice QCD calculations [1], and to study the properties of this matter at extremely high energy densities. A huge number of data have been accumulated and used to extract the information about the original partonic system and its space-time evolution. A variety of experimental facts from various aspects imply that the strongly coupled QGP has been probably produced in central Au+Au collisions at RHIC [2, 3, 4, 5, 6, 7]. Due to the confinement effects, one can only detect the hadrons freed out from the partonic system rather than make direct detection of partons produced in collisions. Therefore, one of the important prerequisites for exploring the quark gluon plasma is the better understanding of hadronization mechanism in nucleus-nucleus collisions.

The quark combination picture is successful in describing many features of multi-particle production in high energy collisions. The parton coalescence and recombination models have explained many highlights at RHIC, such as the high ratio of p/π at intermediate transverse momenta [8, 9, 10] and the quark number scaling of hadron elliptic flows [11, 12, 13]. Our quark combination model has been used to describe the charged particle pseudorapidity densities [14], hadron multiplicity ratios, p_T spectra [15] and elliptic flows [16] at midrapidity.

Recently the STAR collaboration has measured the transverse spectra for identified baryons and mesons in a wider transverse momentum range in central Au+Au collisions at $\sqrt{s_{NN}} = 200$ GeV [17]. The BRAHMS collaboration has given the rapidity spectra [18] and the transverse momentum distributions for identified hadrons at different rapidities [19, 20, 21]. It provides a good opportunity to study the hadron production mechanism in a larger transverse momentum range and at different rapidities. In this paper, we use our quark combination model to study systematically the rapidity and transverse momentum distributions for various hadrons in central Au+Au collisions at $\sqrt{s_{NN}} = 200$ GeV.

The paper is organized as follows. In the next section we

give a brief description of our quark combination model. In section III, the longitudinal and transverse distributions of partons in central Au+Au collisions at $\sqrt{s_{NN}} = 200$ GeV are given. In section IV we compute rapidity distributions of π^\pm , K^\pm , $p(\bar{p})$ and the net proton multiplicity ($p - \bar{p}$), and charged antiparticle-to-particle ratios as a function of rapidity. We predict the rapidity distributions of K_s^0 , $\Lambda(\bar{\Lambda})$, $\Xi^- (\bar{\Xi}^+)$ and $\Omega^- + \bar{\Omega}^+$. In section V we present our results for p_T spectra of π^\pm , K^\pm and $p(\bar{p})$. We also give the p/π ratios in a larger p_T range at $y \sim 0$ and p_T spectra of π^\pm and $p(\bar{p})$ at other rapidities $y \sim 1$, $y \sim 2.2$ and $y \approx 3.2$. Section VI summarizes our work.

II. THE QUARK COMBINATION MODEL

In this section we give a brief description of our quark combination model. The model was first proposed for high energy e^+e^- and pp collisions [22, 23, 24, 25, 26, 27]. It has also been applied to the multi-parton systems in high energy e^+e^- annihilations [28, 29, 30, 31]. Recently we have extended the model to ultra-relativistic heavy ion collisions [14, 15, 16].

The average constituent quark number in nucleus-nucleus collisions can be written as (see e.g. Eq. (4) in Ref. [14])

$$\langle N_q \rangle = 2[(\alpha^2 + \beta \sqrt{s_{NN}})^{1/2} - \alpha] \langle N_{\text{part}}/2 \rangle, \quad (1)$$

where the two parameters are defined by $\beta = 1/2\langle V \rangle$ and $\alpha = \beta m - \frac{1}{4}$. Here $\langle V \rangle$ is the average inter-quark potential. m is the constituent quark mass given by $m = (2m_u + \lambda_s m_s)/(2 + \lambda_s)$, where m_u and m_s are the constituent masses of light and strange quarks respectively, and λ_s is the strangeness suppression factor.

Our quark combination model describes the hadronization of initially produced ground state mesons ($36 - plets$) and baryons ($56 - plets$). In principle the model can also be applied to the production of excited states [24]. These hadrons through combination of constituent quarks are then allowed to decay into the final state hadrons. We take into account the decay contributions of all resonances of $56 - plets$ baryons and $36 - plets$ mesons, and cover all available decay channels by using the decay program of

PYTHIA 6.1 [32]. The main idea is to line up N_q quarks and anti-quarks in a one-dimensional order in phase space, e.g. in rapidity, and let them combine into initial hadrons one by one following a combination rule. See section II of Ref. [15] for short description of such a rule. Of course, we also take into account the near correlation in transverse momentum by limiting the maximum transverse momentum difference Δp_T for quarks and antiquarks as they combine into hadrons. We note that it is very straightforward to define the combination in one dimensional phase space, but it is highly complicated to do it in two or three dimensional phase space [33]. The flavor SU(3) symmetry with strangeness suppression in the yields of initially produced hadrons is fulfilled in the model [22, 24].

III. LONGITUDINAL AND TRANSVERSE DISTRIBUTIONS OF PARTONS

The BRAHMS Collaboration has measured the ratios of antiparticle-to-particle and net-baryon rapidity density ($dN_{(B-\bar{B})}/dy$) as a function of rapidity in central Au+Au collisions at $\sqrt{s_{NN}} = 200$ GeV [34, 35]. The results show that the ratios of K^-/K^+ , \bar{p}/p decrease obviously with increasing rapidity and the $dN_{(B-\bar{B})}/dy$ appears a valley shape in midrapidity region. This suggests that the rapidity distribution of net-quarks is different from that of newborn quarks. In this paper, we describe the momentum distributions of newborn quarks by using a thermal phenomenology with a nonuniform collective flow. The rapidity distribution of net-quarks is given by three-sources relativistic diffusion model [36, 37].

A. momentum distributions of newborn quarks

We start with the momentum spectrum of quarks radiated by a stationary thermal source with temperature T

$$E \frac{d^3 n_{th}}{d^3 \mathbf{p}} = \frac{d^3 n_{th}}{dy p_T dp_T d\phi} \propto E e^{-E/T}. \quad (2)$$

In the following text we give the spectra in terms of rapidity $y = \tanh^{-1}(p_L/E)$ and transverse momentum p_T .

The rapidity distribution of thermal quarks can be given by integrating Eq. (2) over the transverse components [39]

$$\frac{dn_{th}}{dy} \propto \frac{T^3}{(2\pi)^2} \left(\frac{m^2}{T^2} + \frac{m}{T} \frac{2}{\cosh y} + \frac{2}{\cosh^2 y} \right) \exp \left(-\frac{m}{T} \cosh y \right), \quad (3)$$

where m is taken to be constituent quark mass, i.e., $m = 0.34$ GeV for light quarks/antiquarks and $m = 0.5$ GeV for strange quarks/antiquarks. Temperature of thermal source is taken to be $T = 170$ MeV, consistent with the phase transition temperature ($T \sim 165 - 185$ MeV) from lattice QCD calculations.

The momentum distribution of final-state hadrons measured is anisotropic in high energy collisions. It rather has

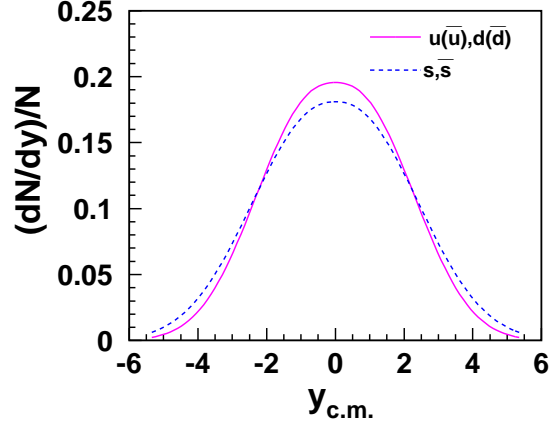


FIG. 1: (Color online) Rapidity spectra of quarks and antiquarks at hadronization in central Au+Au collisions at $\sqrt{s_{NN}} = 200$ GeV.

TABLE I: Normalized expansion functions $w(y)$ for light and strange quarks and antiquarks in central Au+Au collisions at $\sqrt{s_{NN}} = 200$ GeV.

$u, \bar{u} \text{ and } d, \bar{d}$	$w(y) = 0.2 \exp(- y ^{2.62}/14.85)$
s, \bar{s}	$w(y) = 0.184 \exp(- y ^{2.4}/14.85)$

imprinted on the direction of the colliding nuclei. The boost-invariant longitudinal expansion scenario [38, 39] has explained such an anisotropy in terms of a boost-invariant longitudinal flow of matter with locally thermalized distribution. We apply the longitudinal flow to the parton level by adding up the spectra of individual thermal sources which are distributed in a rapidity region $[y'_{min}, y'_{max}]$. Similar to nonuniform longitudinal flow at hadron level [40], we speculate that the individual thermal sources are nonuniformly distributed in the rapidity region. The simplest way to describe this nonuniformity is to introduce a phenomenological expansion function $w(y)$ in the following equation

$$\frac{dn}{dy}(y) = N \int_{y'_{min}}^{y'_{max}} dy' w(y') \frac{dn_{th}}{dy}(y - y'). \quad (4)$$

The transverse momentum spectrum of quark is not affected by this operation [39]. The integrity interval is chosen to be $y'_{max} = -y'_{min} = y_{beam}$. N is the normalization constant. In the quark combination model, excluding the influence of resonance decays from final-state π^+ and K^+ rapidity distribution, we get the initially produced π^+ and K^+ rapidity spectra. We further inversely extract the expansion functions $w(y)$ for light and strange quarks and antiquarks, and obtain rapidity distributions of light and strange quarks and antiquarks. The results are shown in

Table I and Fig. 1 respectively.

The transverse momentum spectrum of thermal quarks can be got by integrating Eq. (2) over rapidity using the modified Bessel function K_1 [39]

$$\frac{dn_{th}}{2\pi p_T dp_T} \propto m_T K_1\left(\frac{m_T}{T}\right), \quad (5)$$

which behaves asymptotically like a decreasing exponential $\exp(-m_T/T)$, here transverse mass $m_T = \sqrt{p_T^2 + m^2}$.

Taken into account transverse flow of thermal source, the partons transversely boost by a flow velocity profile $\beta_r(r)$ as a function of transverse radial positions r . $\beta_r(r)$ is parameterized by the surface velocity β_s : $\beta_r(r) = \beta_s (r/R_{max})^n$. The transverse momentum spectrum of expansion thermal source can be described as [39]

$$\frac{dn_{th}}{2\pi p_T dp_T} = N \int_0^{R_{max}} r dr m_T I_0\left(\frac{p_T \sinh \rho}{T}\right) K_1\left(\frac{m_T \cosh \rho}{T}\right), \quad (6)$$

where I_0 is modified Bessel function, and $\rho = \tanh^{-1} \beta_r$ is transverse rapidity. N is the normalization constant. The value of R_{max} is taken to be $R_{max} = 13$ fm [41]. Values of parameters n, β_s for light and strange quarks and antiquarks are extracted from the transverse momentum distributions of π^0 and K_s^0 at midrapidity in our quark combination model.

Partons at high transverse momenta are mainly from the minijets created in initial hard collisions among nucleons. The transverse momentum distribution of minijet partons in the midrapidity region can be parameterized as [10, 42]

$$\frac{dn_{jet}}{2\pi p_T dp_T} = A \left(\frac{B}{B + p_T} \right)^C. \quad (7)$$

The transition point (p_0) from thermal partons to minijet partons in p_T spectra of quarks and antiquarks is determined by the cross point of the two functions in Eq. (6) and Eq. (7). Thermal partons dominate the transverse momentum below p_0 while minijet partons dominate the transverse momentum greater than p_0 . We extract the p_T spectra of quarks and antiquarks from measured π^0 and K_s^0 spectra, then transition point $p_0 = 1.8$ GeV/c is taken. For thermal quarks, We take $n = 0.5$ for light and strange quarks and antiquarks, $\beta_s = 0.45c, 0.56c$ for light and strange quarks/antiquarks respectively. Values of parameters A, B and C for minijet partons are given in Table II. The scattering of minijet partons with thermal partons may lead to some change of the spectra of minijet partons and the smooth spectra around p_0 . Normalized transverse momentum distributions for light and strange quarks and antiquarks at midrapidity in central Au+Au collisions at $\sqrt{s_{NN}} = 200$ GeV are in Fig. 2.

B. rapidity distribution of net-quarks

In this subsection, we use the three-sources relativistic diffusion model (RDM) [36, 37] to describe the rapidity

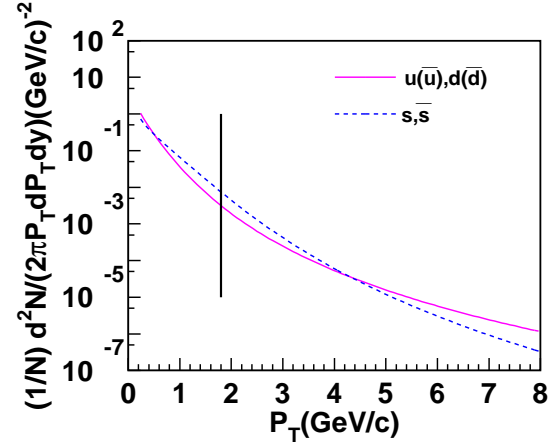


FIG. 2: (Color online) Transverse momentum spectra of quarks and antiquarks at midrapidity in central Au+Au collisions at $\sqrt{s_{NN}} = 200$ GeV. Minijet quarks have transverse momenta $p_T > 1.8$ GeV, while thermal quarks have transverse momenta $p_T < 1.8$ GeV.

TABLE II: Parameters for minijet parton distributions given in Eq.(7) at midrapidity in central Au+Au collisions at $\sqrt{s_{NN}} = 200$ GeV.

	A [1/GeV ²]	B [1/GeV]	C
u, \bar{u} and d, \bar{d}	2.32	1.5	7.25
s, \bar{s}	4.51	1.5	9.5

distribution of net-quarks. The time evolution of distribution functions is given by a Fokker-Planck equation (FPE) in rapidity space [37, 43, 44, 45, 46]

$$\frac{\partial}{\partial t} [R(y, t)]^\mu = -\frac{\partial}{\partial y} [J(y) [R(y, t)]^\mu] + D_y \frac{\partial^2}{\partial y^2} [R(y, t)]^\nu, \quad (8)$$

where $J(y)$ is drift function and D_y is rapidity diffusion coefficient.

Here, we use $q = \nu = 1$ corresponding to the standard FPE, and a linear drift function [37]

$$J(y) = (y_{eq} - y)/\tau_y, \quad (9)$$

where τ_y is rapidity relaxation time, y_{eq} is rapidity equilibrium value and taken to be $y_{eq} = 0$ for symmetric systems.

For the linear case above, exact solutions of standard FPE originating from $R_{1,2}(y, t = 0) = \delta(y \mp y_{beam})$ can be obtained [47]

$$R_{1,2}(y, t) = \frac{1}{\sqrt{2\pi \sigma_{1,2}^2(t)}} \exp \left[-\frac{(y - \langle y_{1,2}(t) \rangle)^2}{2 \sigma_{1,2}^2(t)} \right], \quad (10)$$

where

$$\begin{aligned} \langle y_{1,2}(t) \rangle &= \pm y_{beam} \exp(-t/\tau_y) \\ \sigma_{1,2}^2(t) &= D_y \tau_y [1 - \exp(-2t/\tau_y)]. \end{aligned} \quad (11)$$

The available net-proton data at AGS (Au+Au collisions at $\sqrt{s_{NN}} = 5$ GeV) and SPS (Pb+Pb collisions at $\sqrt{s_{NN}} = 17$ GeV) are reproduced well with a superposition of two sources $R_{1,2}(y, t)$ in RDM. But it has been proposed in Ref. [43] that an expanding midrapidity source $R_3(y)$ emerges at RHIC. With this conjecture, the rapidity distribution of net-quarks in Au+Au collisions at $\sqrt{s_{NN}} = 200$ GeV can be written as [36, 37, 43]

$$\frac{dN(y, t = \tau_{int})}{dy} = N_1 R_1(y, \tau_{int}) + N_2 R_2(y, \tau_{int}) + N_{mid} R_3(y) \quad (12)$$

with the total number of net-quarks $N_1 + N_2 + N_{mid}$ equal to $3N_{part}$. Here τ_{int} is interaction time. The first and second items give the prediction of rapidity distribution for net-quarks at large rapidity, while the last $R_3(y)$ describes the rapidity distribution of net-quarks in the midrapidity region.

There are only two adjustable parameters τ_{int}/τ_y and $D_y\tau_y$ in $R_{1,2}(y, \tau_{int})$. τ_{int}/τ_y represents the diffusive time evolution of net-quarks; $D_y\tau_y$ accounts for the widening of the rapidity distributions due to interactions among partons and partonic creations. In the present paper, $D_y\tau_y$ has included the enhancement factor $g(\sqrt{s})$ caused by memory and collective effects [37, 48, 49]. In central Au+Au collisions at $\sqrt{s_{NN}} = 200$ GeV, values for parameters are taken to be $\tau_{int}/\tau_y = 0.263$ and $D_y\tau_y = 0.9$ respectively.

The stationary solution of Eq.8 is approximate to Gaussian distribution [47]. It is regarded as $R_3(y)$ to describes the midrapidity valley for net-baryon rapidity distribution in Ref.[36, 37, 43]. Instead, for a better description of rapidity distribution of net-quarks, we obtain $R_3(y)$ by fitting the data of net-baryon in our model. The normalized polynomial fit for $R_3(y)$ in a rapidity region $-y_{beam} < y < y_{beam}$ is

$$R_3(y) = 0.0715376 - 0.0189521y^2 - 0.004336y^4 + 0.0000424407y^6 + 0.01001|y| + 0.0194476|y|^3. \quad (13)$$

The rapidity distribution of net-quarks in central Au+Au collisions at $\sqrt{s_{NN}} = 200$ GeV is shown in Fig. 3. Values of N_1, N_2, N_{mid} are taken to be $N_1 = N_2 = 214$ and $N_{mid} = 607$ for central Au+Au collisions at $\sqrt{s_{NN}} = 200$ GeV.

IV. RAPIDITY DISTRIBUTIONS OF IDENTIFIED HADRONS

In this section, we use the quark combination model to compute the rapidity distributions of identified hadrons in central Au+Au collisions at $\sqrt{s_{NN}} = 200$ GeV. The total number of constituent quark is given in Eq.(1). The values of parameters λ_s and β in Eq.(1) are taken to be $\lambda_s = 0.55, \beta = 0.36 \text{ GeV}^{-1}$ respectively [14, 15]. The rapidity distributions of newborn quarks and net-quarks are given respectively in Eq. (4) and Eq. (12). The number of net-quarks is $3N_{part}$ and all the net-quarks are allowed to

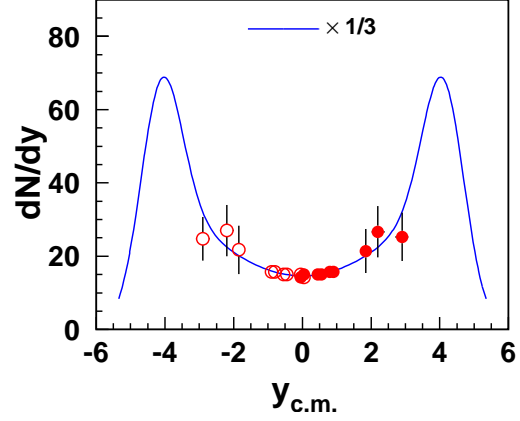


FIG. 3: (Color online) Rapidity distribution of net-quarks in central Au+Au collisions at $\sqrt{s_{NN}} = 200$ GeV. The spectrum is multiplied by 1/3 to compare with the net-baryon data from BRAHMS Collaboration [35].

take part in combination. Minijet partons are indispensable to hadron productions at large transverse momenta. But from the transverse momentum spectra of partons at midrapidity in Fig. 2, we can see that the amount of minijet partons is about two order of magnitude smaller than that of thermal partons. The contribution from minijet partons to the yields and rapidity distributions of hadrons is negligible. Therefore, we don't distinguish between minijet and thermal partons in rapidity. With this input, we can calculate the rapidity distributions of various hadrons.

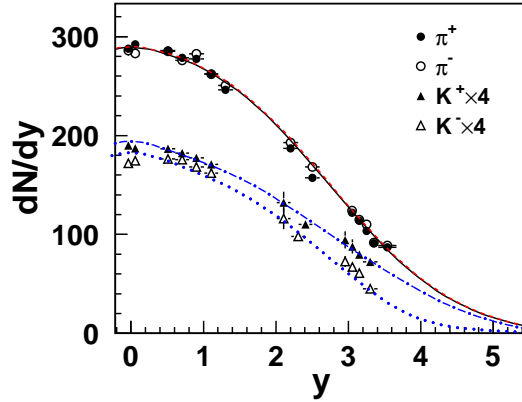


FIG. 4: (Color online) Pions and kaons rapidity densities as a function of rapidity in central Au+Au collisions at $\sqrt{s_{NN}} = 200$ GeV. The kaons yields were multiplied by 4 for clarity. The solid, dashed, dotted-dashed, dotted lines are our results for π^+ , π^- , K^+ and K^- respectively. The experimental data are given by BRAHMS Collaboration [18].

In Fig.4, we show the rapidity distributions of charged pions and kaons in central Au+Au collisions at $\sqrt{s_{NN}} = 200$ GeV. The pion yields are collected excluding the con-

tribution of hyperon (Λ) and neutral kaon K_s^0 decays. In quark combination picture, the existence of net-quarks will lead to the excess of direct produced K^+ over K^- yields, and decay contributions from other particles (K^{*0} , ϕ , Ω) hardly make change to this excess. Therefore the excess of K^+ over K^- yields appears in the full rapidity range. While the directly produced π^+ and π^- yields can not reflect the influence of net quarks. Even if the decay contributions from other hadrons are considered, the difference between yields of π^+ and π^- is also very small compared with the large yields of pions. Thus the rapidity densities of π^+ and π^- are nearly equal within the entire rapidity region. One can see that our model well describes the rapidity densities dN/dy of pions and kaons in the rapidity range covered for central Au+Au collisions at $\sqrt{s_{NN}} = 200$ GeV.

The rapidity distribution of net-proton can reflect the energy loss of colliding nuclei and the degree of nuclear stopping. We calculate the rapidity distributions of proton, antiproton, and net-proton in central Au+Au collisions at $\sqrt{s_{NN}} = 200$ GeV. The results are shown in Fig.5. No weak decay correction has been applied. The existence of net quarks also leads to the excess of directly produced proton over antiproton yields. Taken into account the decay contributions from hyperons, this excess will further increase. Our quark combination model can also successfully explain the data of proton, antiproton, and net-proton in the rapidity region $0 < y < 3$.

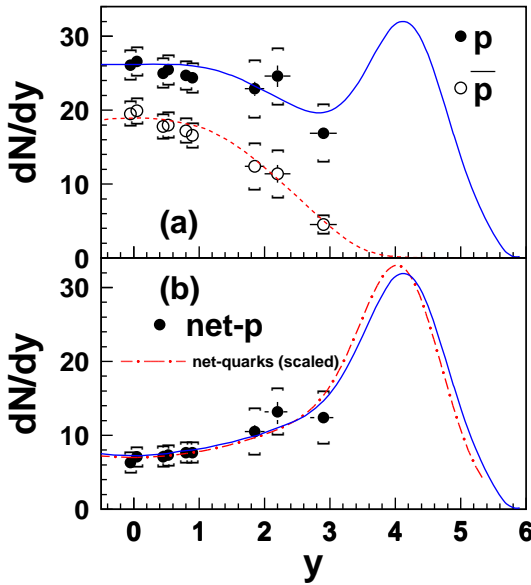


FIG. 5: (Color online) Proton, antiproton and net-proton rapidity densities dN/dy as a function of rapidity in central Au+Au collisions at $\sqrt{s_{NN}} = 200$ GeV. The solid and dashed lines in (a) are our results for proton, antiproton respectively, the solid line in (b) is our result for net-proton. The spectrum of net-quarks scaled is compared with that of net-proton. The errors shown with caps include both statistical and systematic. The experimental data are given by BRAHMS Collaboration [18].

The process of quarks combination is a conversion

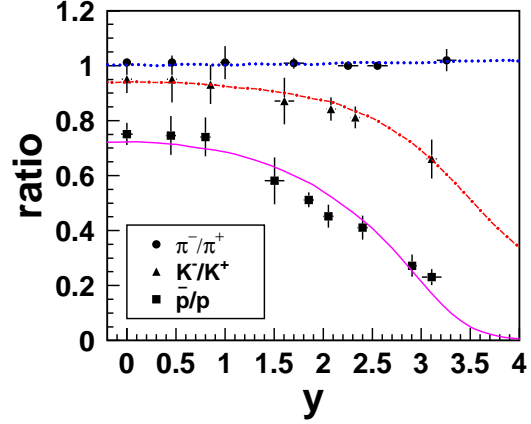


FIG. 6: (Color online) Antiparticle-to-particle ratios as a function of rapidity in central Au+Au collisions at $\sqrt{s_{NN}} = 200$ GeV. The dotted, dotted-dashed and solid lines are our results for π^-/π^+ , K^-/K^+ , \bar{p}/p respectively. The experimental data are from BRAHMS Collaboration [34].

process of net-quarks to net-baryons simultaneously. In Fig.5(b), the computed rapidity distribution of net-proton nearly agrees with that of net-quarks except a small change of peak position around $y \approx 4$. This is mainly because of the mass effects in the processes of quarks combination and resonances decays (see Ref. [14] for explanation of this mass effects). Other baryons also have the similar character. On the other hand, the rapidity distributions of hadrons are only slightly affected by rescattering in late stage of collisions [50]. Therefore, if quark combination mechanism is also applicable to large rapidity region, the measured net-baryon ($B - \bar{B}$) rapidity distribution will reflect quite truly the rapidity distribution of net-quarks just before hadronization. This provides a very beneficial condition to study the energy loss of colliding nuclei and the degree of nuclear stopping in nucleus-nucleus collisions at RHIC.

Rapidity dependence of the ratios for antiparticles to particles are significant indicators of the dynamics of high energy nucleus-nucleus collisions [51, 52]. Since we have computed the rapidity spectra of charged pions, kaons, proton and antiproton, it is convenient to compute the ratios of yields of antiparticles to particles varied with rapidity. In Fig.6, we show the π^-/π^+ , K^-/K^+ and \bar{p}/p ratios as a function of rapidity in central Au+Au collisions at $\sqrt{s_{NN}} = 200$ GeV. No weak decay correction has been applied. The ratio of π^-/π^+ is consistent with unity over the entire rapidity range, while the ratios of K^-/K^+ and \bar{p}/p decrease with increasing rapidity due to the influence of net quarks. Our results agree well with the data.

From the above results, one can see that our model can well describe the rapidity distributions of primary charged hadrons. Among hadrons combined by light and strange quarks and antiquarks, the productions of hyperons Ξ and Ω are less influenced by the decays of other hadrons, thus their rapidity distributions can reflect more directly the

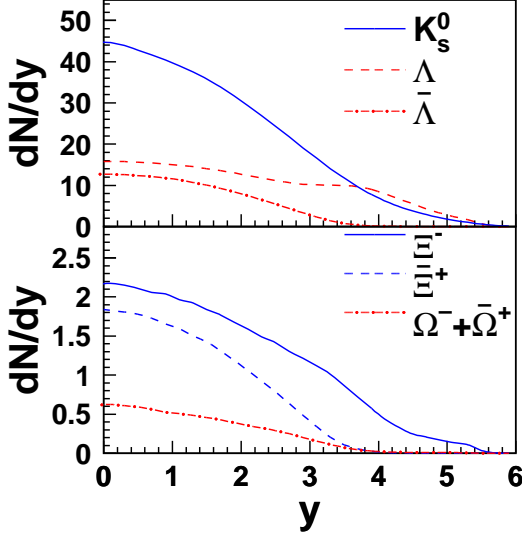


FIG. 7: (Color online) Rapidity distributions for neutral kaon K_s^0 and hyperons $\Lambda(\bar{\Lambda})$, $\Xi^- (\bar{\Xi}^+)$, $\Omega^- + \bar{\Omega}^+$ in central Au+Au collisions at $\sqrt{s_{NN}} = 200$ GeV.

TABLE III: Rapidity densities dN/dy for neutral kaon K_s^0 and hyperons $\Lambda(\bar{\Lambda})$, $\Xi^- (\bar{\Xi}^+)$, $\Omega^- + \bar{\Omega}^+$ at midrapidity in central Au+Au collisions at $\sqrt{s_{NN}} = 200$ GeV. The value of K_s^0 is the fit result according to its transverse momentum spectrum given by STAR Collaboration [53], other data are from STAR Collaboration [54].

	data	our model
K_s^0	45.28*	44.1
Λ	$16.7 \pm 0.2 \pm 1.1$	15.9
$\bar{\Lambda}$	$12.7 \pm 0.2 \pm 0.9$	12.5
Ξ^-	$2.17 \pm 0.06 \pm 0.19$	2.13
$\bar{\Xi}^+$	$1.83 \pm 0.05 \pm 0.2$	1.76
$\Omega^- + \bar{\Omega}^+$	$0.53 \pm 0.04 \pm 0.04$	0.59

hadronization mechanism. We predict the rapidity spectra of neutral kaon K_s^0 and hyperons $\Lambda(\bar{\Lambda})$, $\Xi^- (\bar{\Xi}^+)$, $\Omega^- + \bar{\Omega}^+$ in central Au+Au collisions at $\sqrt{s_{NN}} = 200$ GeV. The results are shown in Fig.7. We also compute the rapidity densities of these hadrons in midrapidity region and compare the results with the experimental data. The data and calculation results are in Table III.

V. RAPIDITY DEPENDENCE OF TRANSVERSE MOMENTUM SPECTRA FOR IDENTIFIED HADRONS

In this section, we calculate p_T spectra of pions, kaons, protons and the p/π ratios in a larger p_T range at $y \sim 0$ in central Au+Au collisions at $\sqrt{s_{NN}} = 200$ GeV. We further compute the transverse momentum distributions of identi-

fied hadrons at other rapidities $y \sim 1$, $\eta = 2.2$ and $y \approx 3.2$.

The transverse momentum distributions of newborn quarks and antiquarks have been given in section III. Based on the experimental fact that π^-/π^+ and \bar{p}/p ratios at midrapidity are almost constants within a broad transverse momentum region [17], the transverse momentum distribution of net-quarks is taken the same as that of newborn light quarks at midrapidity. We use $\Delta p_T = 0.66$ GeV for mesons and $\Delta p_T = 1.0$ GeV for baryons respectively. With this input, we can compute the transverse momentum distributions of various hadrons.

A. Transverse momentum distributions of identified hadrons in a wider p_T range at $y \sim 0$

Identified baryon and meson distributions at large transverse momenta are available in Au+Au collisions at $\sqrt{s_{NN}} = 200$ GeV [17]. It allows one to explore the particle production mechanism in a larger transverse momentum range. In this subsection, we compute the transverse spectra of identified hadrons at large p_T and study the applicable extent of combination mechanism in a larger transverse momentum range.

In Fig.8, we show transverse momentum spectra of π^0 and K_s^0 at midrapidity in central Au+Au collisions at $\sqrt{s_{NN}} = 200$ GeV, which are used to determine the values of parameters for parton p_T spectra. No decay corrections are applied to data. The transverse momentum spectra of pions, kaons, proton and antiproton are calculated at midrapidity in central Au+Au collisions at $\sqrt{s_{NN}} = 200$ GeV. The results are in Fig.9. The pions spectra are corrected to remove the feed-down contributions from K_s^0 and Λ . The feed-down contributions from Λ and Σ^+ are subtracted from the proton spectrum. Our quark combination model can also well explain the data in a large p_T range.

Recently the STAR Collaboration has measured the p/π^+ and \bar{p}/π^- ratios at large transverse momenta in central Au+Au collisions at $\sqrt{s_{NN}} = 200$ GeV, and compared the data with the predictions of recombination and coalescence model [17]. It is found that p/π^+ and \bar{p}/π^- ratios peak at $p_T \sim 2-3$ GeV with values close to unity, decrease with increasing p_T , and approach $p/\pi^+ \approx 0.4$, $\bar{p}/\pi^- \approx 0.25$ at $p_T \gtrsim 7$ GeV. These models can qualitatively describe the $p(\bar{p})/\pi$ ratio at intermediate p_T but in general underpredict the results at high p_T [17]. We also compute the p/π^+ and \bar{p}/π^- ratios in the range $p_T < 12$ GeV. The calculation results are shown in Fig.10. Our results agree with the experimental data in the full p_T range.

One can see from the above results that the quark combination model can reproduce the productions of identified hadrons quite well in a larger transverse momentum range. It suggests that quark combination mechanism may still play an important role at high transverse momentum up to 12 GeV/c.

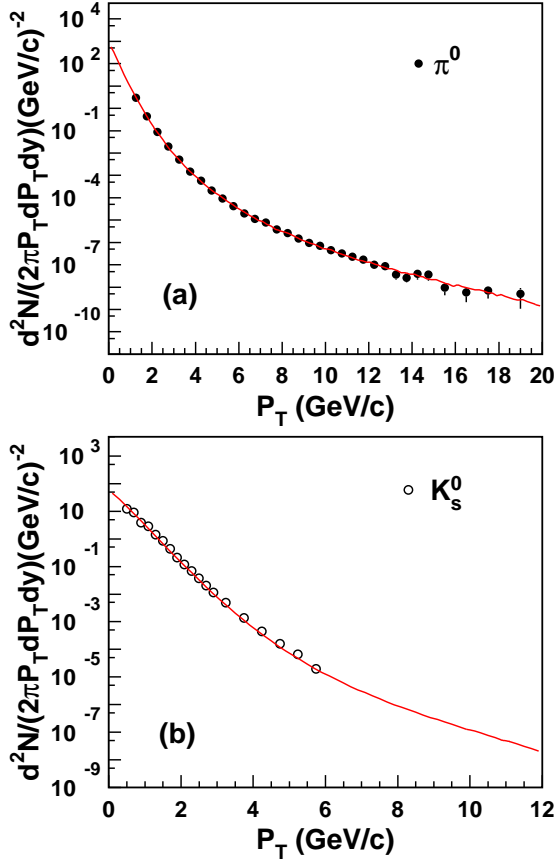


FIG. 8: (Color online) Transverse momentum spectra of π^0 (a), K_s^0 (b) at midrapidity in central Au+Au collisions at $\sqrt{s_{NN}} = 200$ GeV. The solid lines are our results. The data of π^0 are given by PHENIX Collaboration [55], and data of K_s^0 are from STAR Collaboration [53].

B. Transverse momentum spectra of hadrons at other rapidities $y \sim 1$, $\eta = 2.2$ and $y \approx 3.2$

A variety of experimental facts at RHIC indicate that the QGP has been probably produced at midrapidity. Based on this indication, quark combination picture has successfully explained the hadron production at midrapidity [15, 42, 56]. However, can the QGP extend to forward rapidity? If it does, how much rapidity can it extend to? Can combination picture describe the hadron production at forward rapidity yet? Fortunately, the BRAHMS Collaboration recently has measured the p_T spectra of identified hadrons at different rapidities [19, 20, 21]. It provides an opportunity to study the hadrons production at different rapidities and rapidity dependence of hadrons transverse momentum spectra. We have described the longitudinal distributions of identified hadrons in section IV. The transverse momentum spectra of hadrons at midrapidity are well reproduced in the above subsection. We now make a straightforward extension to the forward rapidity region, and this extension should be made with no change

in the quarks p_T spectra before we draw some useful physical information from it.

We compute the transverse momentum spectra of pions and protons at $y \sim 1$ in central Au+Au collisions at $\sqrt{s_{NN}} = 200$ GeV, the results are shown in Fig 11(a). The proton and antiproton spectra are corrected to remove the feed-down contributions from Λ and $\bar{\Lambda}$ weak decays. No significant changes for the transverse spectra of pions and proton(antiproton) are observed within one unit around midrapidity. It suggests that hadrons production at this rapidity are still dominated by combination in intermediate transverse momentum range. The QGP still exist at $y \sim 1$ and it may extend much more than this rapidity.

In Fig 11(b), we show the transverse momentum spectra of pion and antiproton at $\eta = 2.2$ ($2.14 < \eta < 2.26$) in central Au+Au collisions at $\sqrt{s_{NN}} = 200$ GeV. The correction for feed-down from the (anti-)lambda decays has been applied, whereas the contamination of pions due to weak decays has not been corrected. Our model can also well describe the hadronic production at this rapidity.

We further compute the transverse spectra of pions and (anti-)proton at $y \approx 3.2$, the results are shown in Fig 11(c). No correction for decay or feed-down has been applied to data. One can see that computation results are in good agreement with the data for pions, but can't reproduce the data of proton and antiproton. This is probably because the transverse momentum distribution of net-quarks varies with rapidity in nucleus-nucleus collisions at RHIC. The amount of net-quarks is marginal compared with that of newborn quarks in midrapidity region. Net-quarks may be highly thermalized due to interactions with newborn quarks. Its transverse momentum distribution will asymptotically tend to that of newborn light quarks. However the amount of net-quarks can approach and even exceed that of newborn quarks at large rapidity. Therefore the thermalization extent of net-quarks at large rapidity is much smaller than that at midrapidity. Its transverse momentum distribution at large rapidity may be obviously different from that of newborn quarks. Just as analyzed in section IV, the yields of proton and antiproton are more sensitive to the existence of net-quarks than that of pions. Thus the rapidity dependence of transverse momentum distribution for net-quarks should be mainly embodied by that of proton and antiproton, rather than pions. It is one of the probable reason why our quark combination model can describe well the data of pions but for proton and antiproton at $y \approx 3.2$.

From the above results, we can see that the quark combination model is able to describe the transverse momentum distribution of identified hadrons in a broad rapidity range $0 < y < 3.2$. This implies that quark combination hadronization mechanism is still applicable to large rapidity (at least $y = 3.2$). On the other hand, the BRAHMS Collaboration has measured the nuclear modification factor R_{AA} for identified hadrons at forward rapidity in central Au+Au collisions at $\sqrt{s_{NN}} = 200$ GeV [21], and the data also indicate the existence of quark combination mechanism at forward rapidity. The continued suppression seen

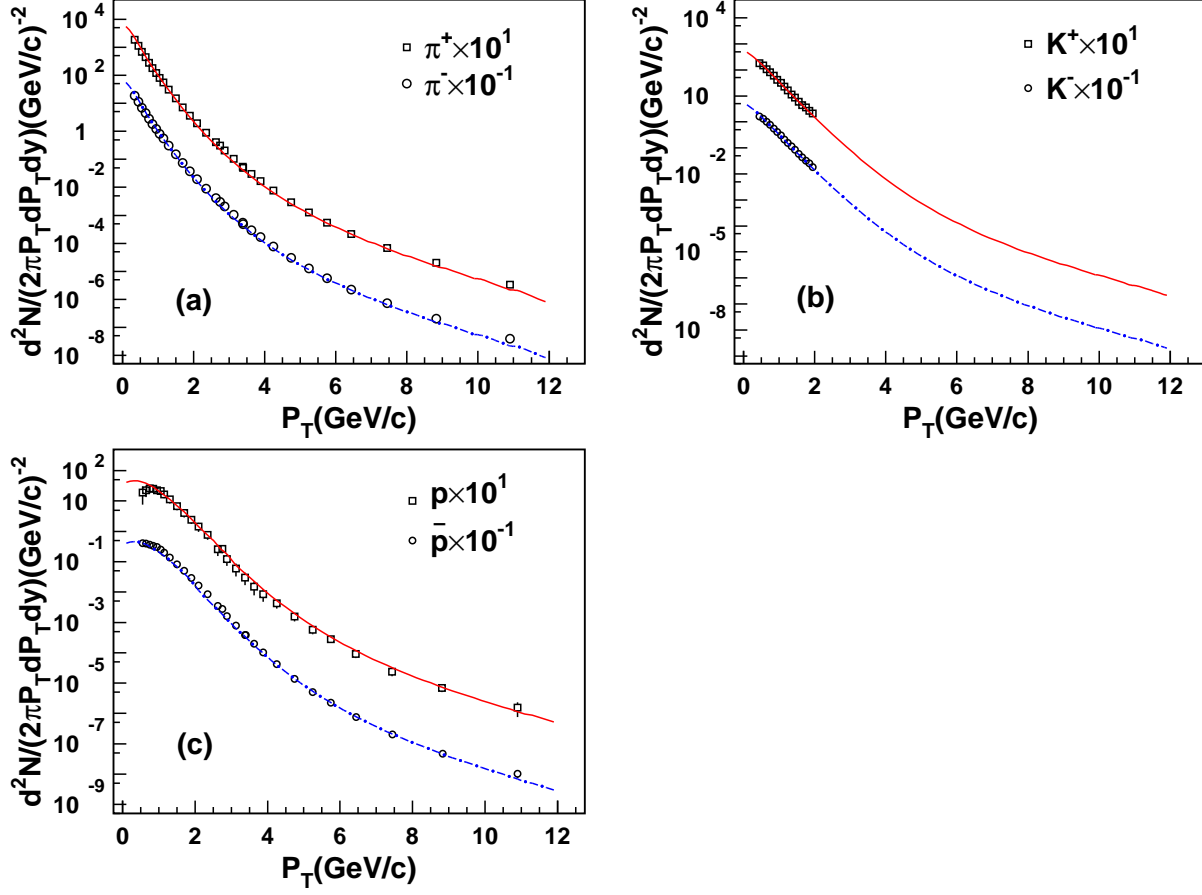


FIG. 9: (Color online) Transverse momentum spectra of pions (a), kaons (b), proton and antiproton (c) at midrapidity in central Au+Au collisions at $\sqrt{s_{NN}} = 200$ GeV. The solid lines are our results for π^+ , K^+ and p , and the dotted-dashed lines are for π^- , K^- and \bar{p} respectively. The data of pions, proton and antiproton are from STAR Collaboration [17], and kaons are from BRAHMS Collaboration [19].

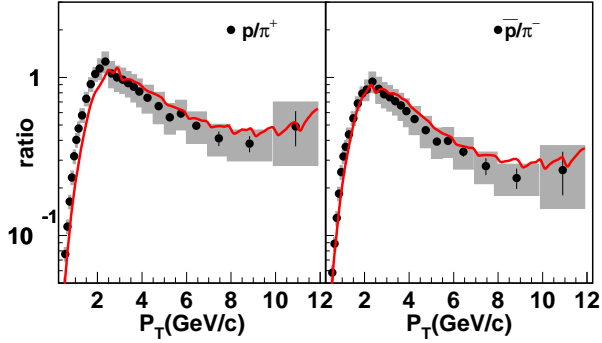


FIG. 10: (Color online) The ratios of p/π^+ and \bar{p}/π^- as a function of transverse momentum at midrapidity in central Au+Au collisions at $\sqrt{s_{NN}} = 200$ GeV. The shaded boxes represent the systematic uncertainties. The solid lines are our results. Experimental data are given by STAR Collaboration [17].

ferent physics from that at midrapidity. The absence of suppression in particle production at large transverse momentum in d+Au collisions shows that the suppression in central Au+Au collisions at midrapidity is not an initial-state effect but a final-state effect of the produced density medium (jet quenching) [57, 58]. However, the initial-state parton saturation effects are more evident at large rapidity [59, 60], which has been testified by the high rapidity suppression measured in d+Au collisions [61]. But the decreasing of the parton medium density at large rapidity will lead to the smaller jet energy loss, thus the less suppression caused by jet quenching can be expected. Therefore the suppression measured at large rapidity in central Au+Au collisions may be the result of a compromise between initial- and final-state effects [62]. Maybe, the same parton p_T spectra at $y = 3.2$ with that at $y = 0$ used in our work is just a synthetic embodiment of the two effects.

in the R_{AA} at $y = 3.2$ further suggests that there is dif-

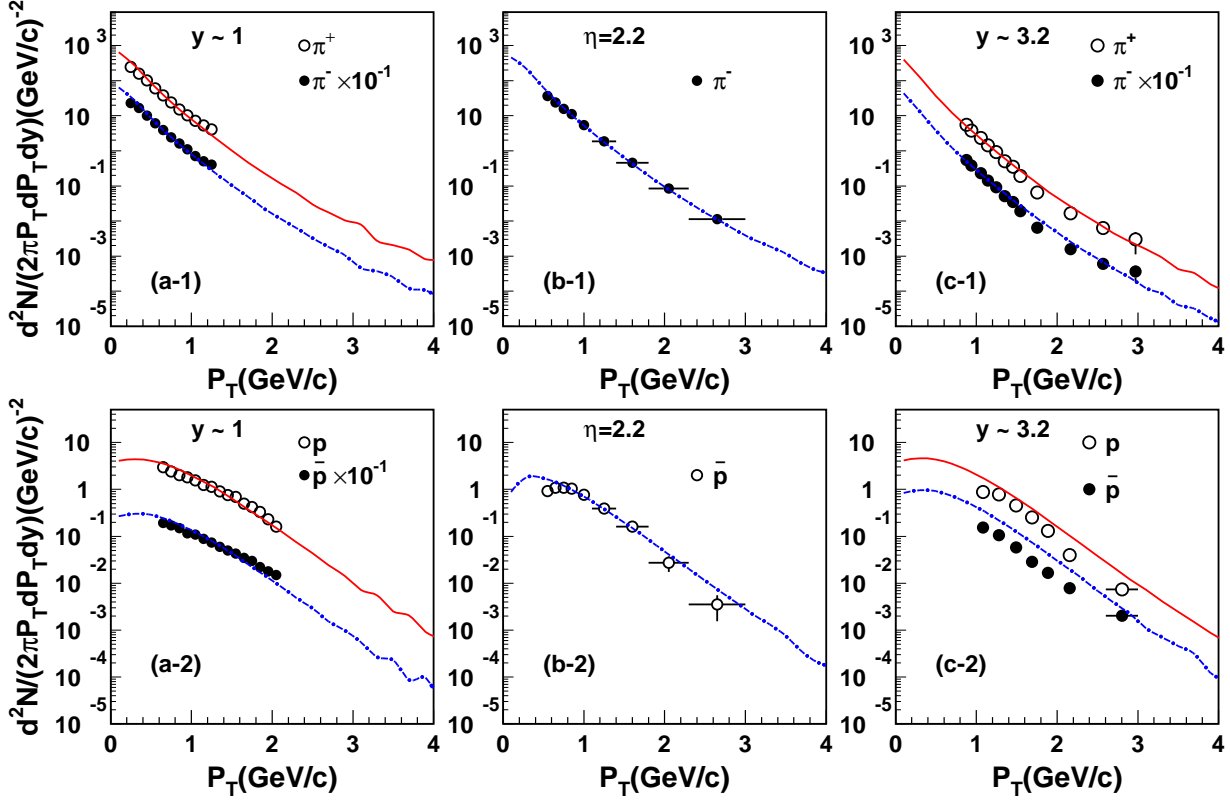


FIG. 11: (Color online) Transverse momentum spectra of pions and protons at $y \sim 1$ (a), $\eta = 2.2$ (b) and $y = 3.2$ (c) in central Au+Au collisions at $\sqrt{s_{NN}} = 200$ GeV. The solid lines are our results for π^+ and p , and the dotted-dashed lines are for π^- and \bar{p} . The data of panel (a),(b),(c) are given by BRAHMS Collaboration [19, 20, 21].

VI. SUMMARY

Using the quark combination model, we study the rapidity and transverse momentum distributions for identified hadrons in central Au+Au collisions at $\sqrt{s_{NN}} = 200$ GeV, incorporating the collective expansion of the hot medium. We use the measured rapidity spectra of π^+ and K^+ to extract the values of parameters and the explicit form of the nonuniform expansion function. The rapidity distributions of net-quarks are described by a relativistic diffusion model [37]. We compute the rapidity distributions of identified hadrons. The results agree with the experimental data. The existence of net quarks leads to the excess of K^+ over K^- and that of proton over antiproton in full rapidity range. The difference between yields of π^+ and π^- resulting from net-quarks is very small compared to the large yields of pions. We further predict the rapidity spectra of K_s^0 , $\Lambda(\bar{\Lambda})$, $\Xi^- (\bar{\Xi}^+)$ and $\Omega^- + \bar{\Omega}^+$ in central Au+Au collisions at $\sqrt{s_{NN}} = 200$ GeV. We also calculate the transverse spectra of identified hadrons and the ratios of proton/ antiproton to pions in a large transverse momentum

range at midrapidity. Our model reproduces the data quite well, which suggests that combination scenario may still play an important role in hadronization at high p_T up to 12 GeV/c. Finally we give rapidity dependence of transverse momentum spectra of hadrons. Using the same transverse momentum spectra for quarks, we calculate the transverse momentum spectra at various rapidities $y \sim 0, 1$, $\eta = 2.2$ and $y \approx 3.2$. The results are in good agreement with the data except those for proton and antiproton at $y \approx 3.2$.

ACKNOWLEDGMENTS

The authors thank Q. Wang, S.-Y. Li, and Z.-T. Liang for helpful discussions. The work is supported in part by the National Natural Science Foundation of China under the grant 10475049, the foundation of University Doctorate Educational Base of Ministry of Education under the grant 20030422064, and the science fund of Qufu Normal University.

[1] T. Blum *et al.* Phys. Rev. D **51**, 5153 (1995)

[2] J. Adams *et al.* [STAR Collaboration], Nucl. Phys. A **757**,

- 102 (2005)
- [3] M. Gyulassy and L. McLerran, Nucl. Phys. A **750**, 30 (2005)
- [4] P. Jacobs and X. N. Wang, Prog. Part. Nucl. Phys. **54**, 443 (2005)
- [5] P. F. Kolb and U. W. Heinz, arXiv:nucl-th/0305084.
- [6] P. Braun-Munzinger, K. Redlich and J. Stachel, arXiv:nucl-th/0304013.
- [7] D. H. Rischke, Prog. Part. Nucl. Phys. **52**, 197 (2004)
- [8] R. C. Hwa and C. B. Yang, Phys. Rev. C **67**, 034902 (2004)
- [9] V. Greco, C. M. Ko and P. Levai, Phys. Rev. Lett. **90**, 202302 (2003)
- [10] R. J. Fries, B. Muller, C. Nonaka and S. A. Bass, Phys. Rev. Lett. **90**, 202303 (2003)
- [11] S. A. Voloshin, Nucl. Phys. A **715**, 379 (2003)
- [12] D. Molnar and S. A. Voloshin, Phys. Rev. Lett. **91**, 092301 (2003)
- [13] Z. w. Lin and C. M. Ko, Phys. Rev. Lett. **89**, 202302 (2002) [arXiv:nucl-th/0207014].
- [14] F. L. Shao, T. Yao, and Q. B. Xie, Phys. Rev. C **75**, 034904 (2007)
- [15] F. L. Shao, Q. B. Xie and Q. Wang, Phys. Rev. C **71**, 044903 (2005)
- [16] T. Yao, Q. B. Xie and F. L. Shao, arXiv:nucl-th/0606033.
- [17] B. I. Abelev *et al.* (STAR Collaboration), Phys. Rev. Lett. **97**, 152301 (2006)
- [18] I. G. Bearden *et al.* (BRAHMS Collaboration), Phys. Rev. Lett. **94**, 162301 (2004)
- [19] I. Arsene *et al.* (BRAHMS Collaboration), Phys. Rev. C **72**, 014908 (2005)
- [20] I. Arsene *et al.* (BRAHMS Collaboration), arXiv:nucl-th/0610021.
- [21] Radoslaw Karabowicz (for BRAHMS Collaboration) Nucl. Phys. A **774**, 477-480 (2006)
- [22] Q. B. Xie and X. M. Liu, Phys. Rev. D **38**, 2169 (1988)
- [23] Z. T. Liang and Q. B. Xie, Phys. Rev. D **43**, 751 (1991).
- [24] Q. Wang and Q. B. Xie, J. Phys. G **21**, 897 (1995).
- [25] J. Q. Zhao, Q. Wang and Q. B. Xie, Sci. Sin. A **38**, 1474 (1995).
- [26] Q. Wang, Z. G. Si and Q. B. Xie, Int. J. Mod. Phys. A **11**, 5203 (1996).
- [27] Z. G. Si, Q. B. Xie and Q. Wang, Commun. Theor. Phys. **28**, 85 (1997).
- [28] Q. Wang and Q. B. Xie, Phys. Rev. D **52**, 1469 (1995).
- [29] Q. Wang, Q. B. Xie and Z. G. Si, Phys. Lett. B **388**, 346 (1996).
- [30] Q. Wang, G. Gustafson and Q. B. Xie, Phys. Rev. D **62**, 054004 (2000)
- [31] Q. Wang, G. Gustafson, Y. Jin and Q. B. Xie, Phys. Rev. D **64**, 012006 (2001)
- [32] T. Sjostrand, P. Eden, C. Friberg, L. Lonnblad, G. Miu, S. Mrenna, and E. Norrbin, Comput. Phys. Commun. **135**, 238 (2001).
- [33] M. Hofmann, M. Bleicher, S. Scherer, L. Neise, H. Stocker and W. Greiner, Phys. Lett. B **478**, 161 (2000).
- [34] I. G. Bearden *et al.* (BRAHMS Collaboration), Phys. Rev. Lett. **90**, 102301 (2003).
- [35] I. G. Bearden *et al.* (BRAHMS Collaboration), Phys. Rev. Lett. **93**, 102301 (2004).
- [36] Rolf Kuiper and Georg Wolschin Annalen Phys. **16**:67-77 (2007)
- [37] G. Wolschin, Phys. Rev. C **69**, 024906 (2004).
- [38] J D Bjorken, Phys. Rev. D **27**, 140 (1983).
- [39] E. Schnedermann, J. Sollfrank, and U. Heinz, Phys. Rev. C **48**, 2462 (1993); E. Schnedermann and U. Heinz, *ibid* **48**, 1675 (1994).
- [40] Feng Shengqin, Liu feng, and Liu Lianshou, Phys. Rev. C **63**, 014901 (2000).
- [41] F. Retière *et al.* nucl-ex/0111013 (2001), F. Retière and M. Lisa, Phys. Rev. C **70** 044907 (2004).
- [42] V. Greco, C. M. Ko and P. Levai, Phys. Rev. C **68**, 034904 (2003)
- [43] G. Wolschin, Phys. Lett. B **569**, 67 (2003).
- [44] W.M. Alberico, A. Lavagno, and P. Quarati, Eur. Phys. J. C **12**, 499 (2000); A. Lavagno, Physica A **305**, 238 (2002).
- [45] M. Rybczyński, Z. Włodarczyk, and G. Wilk, Nucl. Phys. B (Proc. Suppl.) **122**, 325 (2003).
- [46] M. Biyajima, M. Ide, T. Mizoguchi, and N. Suzuki, Prog. Theor. Phys. **108**, 559 (2002).
- [47] G. Wolschin, Eur. Phys. J. A **5**, 85 (1999).
- [48] G. Wolschin, Europhys. Lett. **47**, 30 (1999).
- [49] G. Wolschin, Proc. ICPAQGP, Jaipur (2001): Pramana **60**, 1035 (2003).
- [50] H. Boggild, Ole Hansen, T. J. Humanic, Phys. Rev. C **74** 064905 (2006).
- [51] N. Herrmann *et al.*, Ann. Rev. Nucl. Part. Sci. **49** 581 (1999).
- [52] H. Satz, Rep. Prog. Phys. **63** 1511 (2000).
- [53] J. Admas *et al.* (STAR Collaboration), submitted to Phys. Rev. C, nucl-ex/0601042 (2006).
- [54] J. Admas *et al.* (STAR Collaboration), Phys. Rev. Lett. **98**, 062301 (2006).
- [55] Tadaaki Isobe (PHENIX Collaboration), nucl-ex/0510085 (2005).
- [56] R. C. Hwa and C. B. Yang, Phys. Rev. C **70**, 024905 (2004).
- [57] S. s. Adler *et al.* (PHENIX Collaboration) Phys. Rev. Lett. **91**, 072303 (2003)
- [58] J. Admas *et al.* (STAR Collaboration), Phys. Rev. Lett. **91**, 072304 (2003)
- [59] D. Kharzeev, Y.V. Kovchegov, and K. Tuchin, Phys. Rev. D **68**, 094013 (2003); D. Kharzeev, E. Levin, and L. McLerran, Phys. Lett. B **561**, 93 (2003).
- [60] J. Jalilian-Marian, Y. Nara, and R. Venugopalan, Phys. Lett. B **577**, 54 (2003); A. Dumitru and J. Jalilian-Marian, Phys. Rev. Lett. **89**, 022301 (2002).
- [61] I. Arsene *et al.* (BRAHMS Collaboration), Phys. Rev. Lett. **93**, 242303 (2003)
- [62] R. Debbe for the BRAHMS Collaboration, nucl-ex/0608048, to appear in the proceedings of the 9th Conference on the Intersections of Particle and Nuclear Physics (CIPANP 2006), Puerto Rico, 30 May - 3 June 2006